

Experimental probe of multi-mobility edges in quasiperiodic mosaic lattices

Jun Gao,^{1,*} Ivan M. Khaymovich,^{2,3,†} Xiao-Wei Wang,⁴ Ze-Sheng Xu,¹ Adrian Iovan,¹
Govind Krishna,¹ Alexander V. Balatsky,^{2,5} Val Zwiller,¹ and Ali W. Elshaari^{1,‡}

¹*Department of Applied Physics, KTH Royal Institute of Technology, Albanova
University Centre, Roslagstullsbacken 21, 106 91 Stockholm, Sweden*

²*Nordita, Stockholm University and KTH Royal Institute of Technology, Hannes Alfvéns väg 12, SE-106 91 Stockholm, Sweden*

³*Institute for Physics of Microstructures, Russian Academy of Sciences, 603950 Nizhny Novgorod, GSP-105, Russia*

⁴*Center for Integrated Quantum Information Technologies (IQIT), School of Physics and Astronomy and State Key Laboratory of
Advanced Optical Communication Systems and Networks, Shanghai Jiao Tong University, Shanghai 200240, China*

⁵*Department of Physics, University of Connecticut, Storrs, Connecticut 06269, USA*

(Dated: June 21, 2023)

The mobility edge (ME) is a crucial concept in understanding localization physics, marking the critical transition between extended and localized states in the energy spectrum. Anderson localization scaling theory predicts the absence of ME in lower dimensional systems. Hence, the search for exact MEs, particularly for single particles in lower dimensions, has recently garnered significant interest in both theoretical and experimental studies, resulting in notable progress. However, several open questions remain, including the possibility of a single system exhibiting multiple MEs and the continual existence of extended states, even within the strong disorder domain. Here, we provide experimental evidence to address these questions by utilizing a quasiperiodic mosaic lattice with meticulously designed nanophotonic circuits. Our observations demonstrate the coexistence of extended and localized states in lattices with broken duality symmetry and varying modulation periods. By single site injection and scanning the disorder level, we could approximately probe the ME of the modulated lattice. These results corroborate recent theoretical predictions, introduce a new avenue for investigating ME physics, and offer inspiration for further exploration of ME physics in the quantum regime using hybrid integrated photonic devices.

Disorder-induced localization, a phenomenon initially predicted by P. W. Anderson in 1958 [1], has been a prominent topic in condensed matter physics [2, 3]. The scaling theory of localization [4] revealed that in lower-dimensional disordered systems, all states become localized, whereas in three-dimensional systems, localized and extended eigenstates can coexist, resulting in the existence of a critical energy E_c known as the mobility edge (ME) [5]. Notably, when a quasiperiodic potential replaces random disorder, such as in the Aubry-André (AA) model [6, 7], a distinct picture emerges. This model suggests an energy-independent critical metal-insulator transition at a self-dual point, subsequently confirmed by experiments conducted both on photonic [8] and atomic [9, 10] platforms. However, due to its self-dual symmetry, the AA model does not possess a ME. The existence of MEs

in one-dimensional (1D) systems is primarily conjectured in more generalized models [11–35], serving as a catalyst for numerous experimental investigations based on ultracold atoms [36–38].

Recently, a significant advancement in the field of ME physics has emerged with the introduction of Avila’s global theory [39], one of his *Fields Medal* work. This novel theoretical framework has uncovered a distinct class of exactly solvable 1D models, where quasiperiodic on-site potentials are incorporated with certain periods [40]. Referred to as mosaic lattices, these models exhibit a range of compelling features. Notably, unlike previous models employing random or other quasiperiodic disorders, the mosaic lattice displays the remarkable property of hosting multiple MEs while breaking self-duality symmetry. Moreover, regardless of the strength of the quasiperiodic potential, extended states persist throughout the system — a striking departure from the previous findings.

Here, we conducted experimental implementation of quasiperiodic mosaic lattices using integrated silicon nitride (Si_3N_4) photonic circuits with complementary metal-oxide-semiconductor (CMOS) compatible fabrication technology [41–48]. By precisely engineering the on-site potential of each lattice site and adjusting the in-between gaps, while maintaining uniform hopping terms, we successfully achieved the desired quasiperiodic modulation over a wide tuning range at room temperature. Through single site excitation of the photonic mosaic lattice in the strong tuning regime, we observe clear signatures of multiple MEs, which arise from the energy-dependent coexistence of localized and extended states. The existence of MEs is further confirmed by scanning the quasiperiodic potential strength and probing the average energy of the injected state. Our results showcase the capacity of integrated photonics platforms to investigate ME physics in a scalable and precise manner, with the potential to explore and uncover unique quantum features depending on bosonic coalescence [49–51] in quasiperiodic lattice models.

The Hamiltonian of the quasiperiodic mosaic model can be described as

$$H = J \sum_j \left(c_j^\dagger c_{j+1} + \text{H.c.} \right) + 2 \sum_j \lambda_j n_j. \quad (1)$$

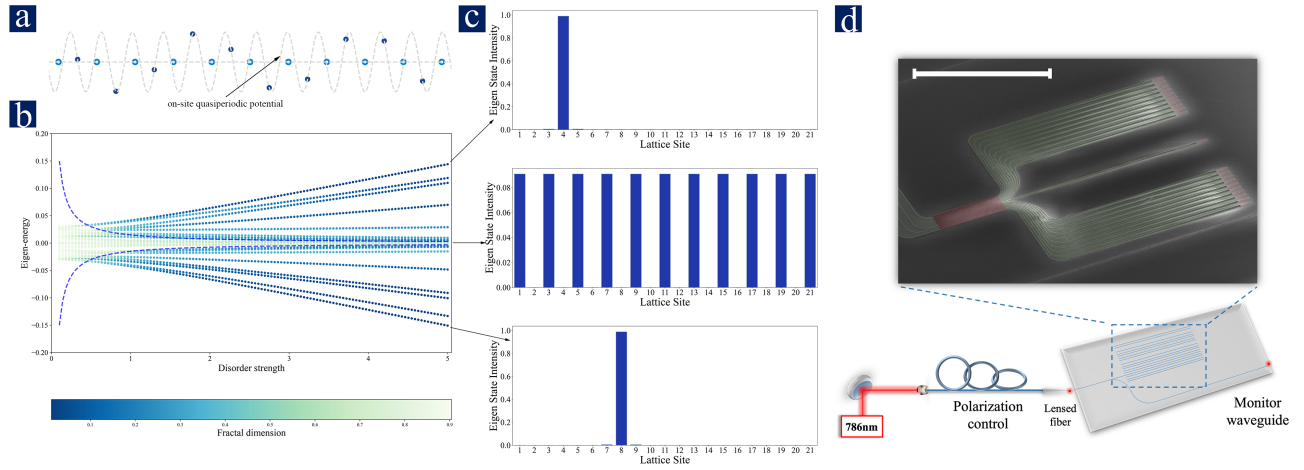


FIG. 1. **Mobility edge in $\kappa = 2$ quasiperiodic mosaic lattice.** (a) Schematic of the 1D quasiperiodic mosaic lattice, exemplifying the mobility edge phenomena in condensed matter physics. For the case of $\kappa = 2$, the energy of every second lattice site is modified in accordance with equation 2, while the hopping constant J between lattice sites is held constant throughout. (b) Energy diagram illustrating the dependence of eigenstate energies on quasiperiodic potential strength (λ). Each data point signifies the energy of a specific eigenstate at a given potential strength, with color coding employed to represent the energy-dependent fractal dimension D_2 . The 1D photonic lattice under investigation comprises 21 sites. (c) Real-space distribution of three distinct eigenstates at a disorder strength $\lambda = 5$: (i) the highest positive energy eigenstate, localized predominantly at site 4; (ii) an extended state near zero energy; and (iii) the highest negative energy eigenstate, localized primarily at site 8. The system exhibits two mobility edges, as described by equation (5), where eigenstates transition from localized to extended upon crossing the mobility edge. (d) Sketch of the experimental setup. A 786nm laser is first prepared in TE mode and then injected into the lattice via a lensed fiber. The figure shows SEM image of the fabricated device. The input waveguide is split into the mosaic lattice and a monitor waveguide. The intensity distribution in the lattice is reflected by the grating couplers (red) and recorded through top imaging.

Here, c_j^\dagger is the creation operator at site j , J is the nearest neighbor hopping term, and λ_j represents the on-site quasiperiodic potential modulation, which is given by the following formula,

$$\lambda_j = \begin{cases} \lambda \cos[2\pi(\omega j + \theta)], & j = \kappa m, \\ 0, & \text{otherwise.} \end{cases} \quad (2)$$

θ is the phase offset during the modulation, ω is an irrational number, for instance $(\sqrt{5} - 1)/2$ in our case, and κ is an integer determining the mosaic modulation period. When $\kappa = 1$, the lattice reduces to the AA model with self-dual symmetry and transition at $\lambda = 1$, whereas when $\kappa \neq 1$, the duality symmetry of the lattices is broken. Fig. 1(a) demonstrates a 1D quasiperiodic mosaic model with $\kappa = 2$ modulation period. In our simulation and experimental design, we set $\theta = 0$ for the convenience, and $J = 0.015$ enabling wide tuning range of the potential amplitude modulation λ .

Following Avila's profound global theory [39], it has been theoretically proved [40] that the mosaic model indeed manifests energy-dependent MEs by computing the Lyapunov exponent (see Supplementary Information for details), which can be described by the following expression:

$$|\lambda a_\kappa| = J \quad \text{for} \quad E = E_c, \quad \text{with} \quad (3)$$

$$a_\kappa = \frac{\sin(\kappa p)}{\sin p}, \quad E = 2J \cos p \quad (4)$$

the parametrization of the energy E via the real (imaginary)-valued momentum p for $|E| \leq 2J$ ($|E| > 2J$). A mosaic lattice with κ modulation period hosts $2(\kappa - 1)$ MEs, which are distributed in energy spectrum around $E = 2J \cos(\pi m/\kappa)$, where $a_\kappa = 0$ and the extended states survive at arbitrarily strong potential λ , which is a new fundamental feature of mosaic lattices (see Supplementary Information A.1). For the simplest yet nontrivial case of $\kappa = 2$, the two MEs are given by

$$E_c = \pm J/\lambda. \quad (5)$$

In Fig. 1(b) we show the calculated eigenvalues of a 21-site lattice versus the modulation strength λ based on our chosen parameters. To characterize the MEs, we utilize the fractal dimension [5], defined $D_2 = -\lim_{L \rightarrow \infty} [\ln \langle \text{IPR} \rangle / \ln L]$ via the inverse participation ratio $\text{IPR} = \sum_j |\psi_i(j)|^4$ of eigenstates $\psi_i(j)$, averaged over the energies E_i , to distinguish extended ($D_2 \rightarrow 1$) and localized states ($D_2 \rightarrow 0$). The dashed blue lines represent the exact MEs for $\kappa = 2$ mosaic lattice as the transition between $D_2 = 0$ and 1.

In Fig. 1(c), we showcase three distinct eigenstates intensity distribution at a disorder level of $\lambda = 5$. We could see the spatial distributions of the wave functions are exponentially localized at disordered sites $j = \kappa m$ (shown for the highest and lowest energy). For the extended eigenstate, the particle tends to stay at the sites without potential modulation (see Supplementary Information A.2), this also explains the survival of extended states in the mosaic lattice at strong

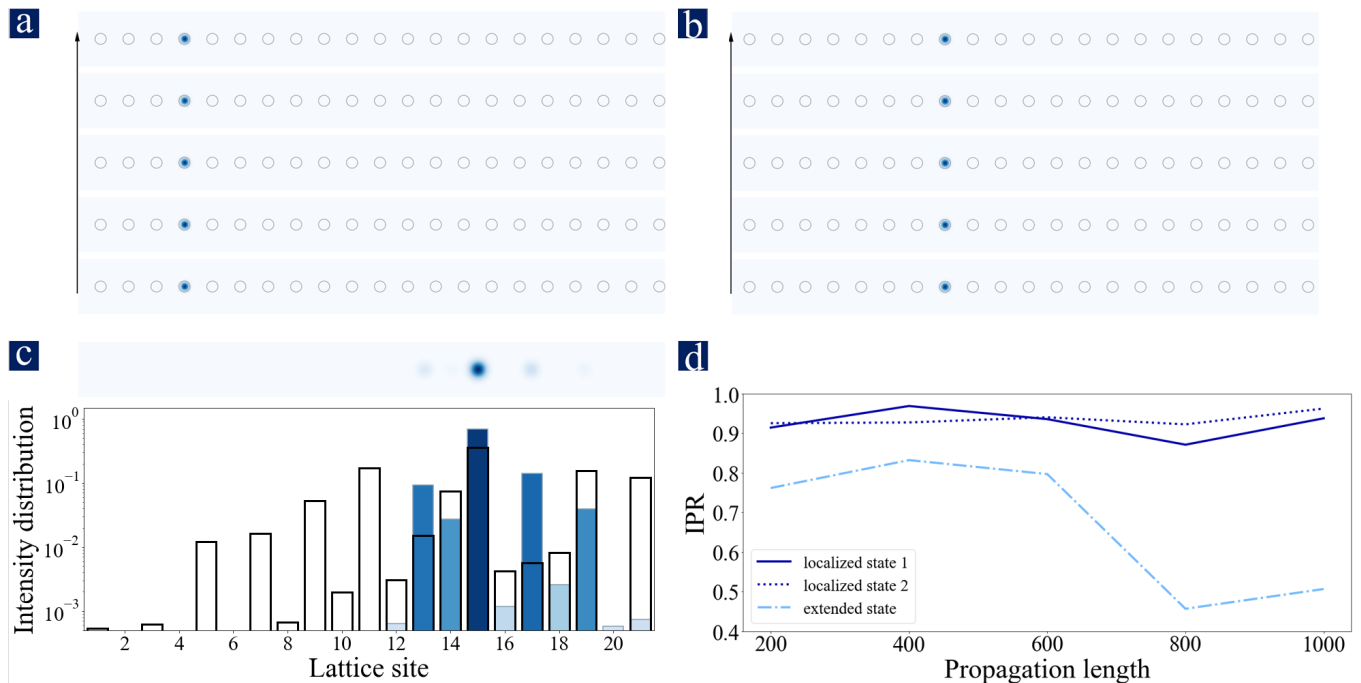


FIG. 2. **Experimental probe of localized and extended states in $\kappa = 2$ mosaic lattice.** (a) Real-space distribution of light intensity probed every $200\mu\text{m}$ along the lattice, with light injected at lattice site 4. The observed confinement of light primarily at site 4 with minimal spreading to neighboring waveguides indicate the strong localization due to overlap with the localized highest positive energy eigenstate depicted in Fig. 1(c). (b) Similar measurement for light injected at waveguide 8, corresponding to the highest negative energy localized eigenstate depicted in Fig. 1(c). The observed localization of light, consistent with the behavior described in Fig. 2(a), emphasizes the strong overlap with the localized states. (c) Real-space distribution of light intensity for light injected at site 15, exhibiting significant wave-packet spreading. Bar plot below shows the light intensity on a logarithmic scale, measured after $1000\mu\text{m}$ of light propagation in the lattice. Unfilled bars represent simulation results and colored bars indicate experimental measurements. (d) Inverse participation ratio (IPR) calculated for the three wave packets, presented in Figs. 2(a), (b), and (c). Single-site excitations, overlapping strongly with localized states, maintain a high level IPR for varying propagation lengths, while the one, overlapping with an extended state, as in Fig. 2(c), exhibits IPR reduction with the propagation distance. This behavior confirms the ME presence for a specific potential strength λ .

potential.

Experimentally, we implement the photonic quasiperiodic mosaic lattices based on integrated Si_3N_4 photonics platform (see Supplementary Information B for more fabrication details) [52]. A scanning electron microscope (SEM) image of the nanophotonic device is presented in Fig. 1(d). To design the desired on-site potential of each modulated site, we control the width of each waveguide according to numerical vectorial mode solver [53]. We set 550 nm as the default width for a flexible tuning range while maintaining single-mode profile operation, and the modulated sites are designed to yield the potential modulation at a given modulation level of $\lambda = 5$, shown in Supplementary Information A.1 to be enough to form all the MEs. The waveguide separation is carefully designed to keep the hopping term uniform due to the asymmetric coupling of different waveguide widths (see Supplementary Information C for the design methods). We choose the 4th, 8th and 15th inputs to probe different regimes in the energy diagram. We adiabatically expand the output array by a fan-out structure, and all the output waveguides are coupled to grating couplers for the spatial intensity measurement. An additional monitor waveguide is

fabricated for the facet beam profile imaging and polarization control as our previous designs [54–56]. We also vary the propagation lengths in the samples from 200 to $1000\mu\text{m}$ with an interval of $200\mu\text{m}$ to probe the light dynamics in the lattices.

The schematic of the experimental setup is shown in Fig. 1(d). The photonic quasiperiodic mosaic lattice is probed using a coherent laser at a wavelength of 786 nm , which is prepared with horizontal polarization (TE mode). The light is coupled to the lattice through a lensed fiber mounted on a 6-axis nano-positioning stage (Thorlabs NanoMax). The input waveguide is divided into two paths: one serves as a monitor waveguide for polarization control, while the other leads to the injection site. The output intensity is top-imaged using a $40\times$ objective and directly measured by a charge-coupled device (CCD) camera that records the reflected light from the grating couplers. An example of image acquisition can be found in the Supplementary Information Fig. S3.

We first probe the two localized states in $\kappa = 2$ photonic mosaic lattice. Figs. 2(a) and (b) present the top images of light intensity distribution of localized states every $200\mu\text{m}$ along the propagation distance. The grey circles mark the

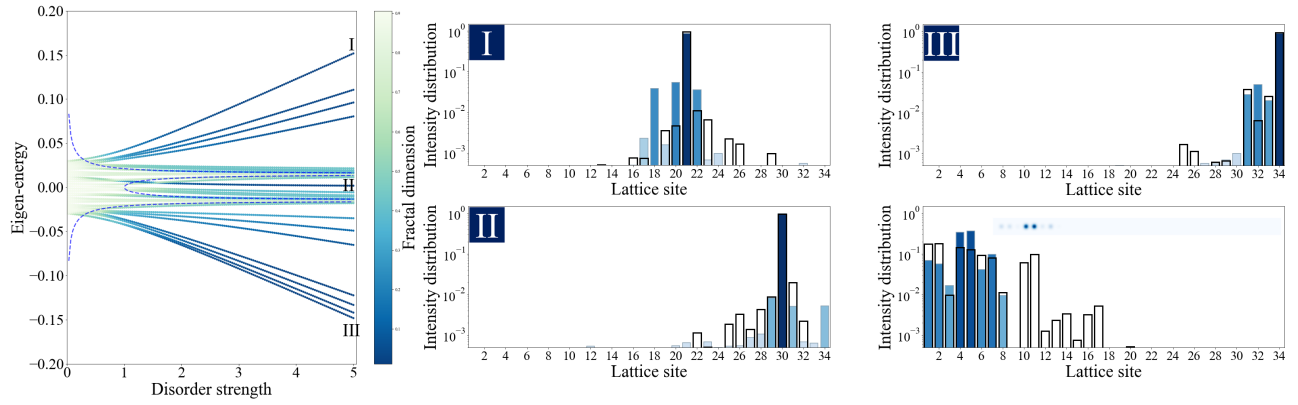


FIG. 3. **Experimental probe of $\kappa = 3$ mosaic lattice of 34 sites.** (left) Eigenvalue evolution with increasing quasiperiodic disorder strength λ . Each point represents the energy of an individual eigenstate, color coded by the corresponding fractal dimension. As the disorder strength increases, the system develops four MEs, separating three localization regimes **I**, **II**, **III**, see labeled panels, with two extended eigenstates regimes in between highlighted by a fractal dimension approaching unity. Propagation of a single-site excitation probes different regimes of the energy spectrum at a disorder strength of $\lambda = 5$. The eigenstates distributions in real space and their overlap with the corresponding choice of single site excitation are given in the **Supplementary Information E**. **I**, **II**, **III** present the output spatial distribution of the light intensity in a logarithmic scale after propagating $1000 \mu\text{m}$ in the lattice, using single-site excitation at the 21st, 30th, and 34th waveguide, respectively. Unfilled bars represent simulation results and colored bars indicate experimental measurements, with the color code highlighting the light intensity. The experiment shows good agreement with the simulation, where the light is exponentially localized in the excitation lattice site. (bottom right) Experimental and numerical intensity distribution after propagating $1000 \mu\text{m}$ in the lattice for a single-site excitation at the 4th lattice site, overlapping with the extended eigenstates in the energy spectrum. More spreading of light highlights delocalization transition in the eigenstate spectrum, thus, exhibiting a ME. The inset shows the measured experimental distribution in a linear scale.

position of every site in the lattice. The figures clearly show the strong spatial confinement of the injected light at site 4 and site 8. These two excitation cases correspond to the highest and lowest energy eigenstates, shown in Fig. 1(c). As a comparison, we also excite the 15th site to probe an extended state in the lattice. Fig. 2(c) illustrates the light intensity distribution in the lattice over a propagation distance of $1000 \mu\text{m}$ with both linear (top) and logarithmic (bottom histogram) scale, confirming mostly odd-site occupancy. To quantify the transport behavior, we calculate the IPR values for spreading wave-packets in all three cases versus propagation distance. The IPR values in Fig. 2(d) for the localized cases remain close to 1 as the propagation length increases, while the IPR value for the extended state shows the expansion of the initial single-site wave packet (see Supplementary Information A.3). Our measurements provide experimental evidence of energy-dependent localization phase transition in the mosaic model.

Then, we investigate the $\kappa = 3$ photonic mosaic lattice comprising 34 sites at the same modulation strength. The lattice contains four MEs given by the expression of $E_c = \pm J\sqrt{1 \pm 1/\lambda}$. The corresponding energy diagram is depicted in Fig. 3, where the four MEs have divided the spectrum into various regions. Here, we mark three distinct localized eigenstates as **I**, **II**, and **III** (see Supplementary Information E for intensity distributions of $\kappa = 3$ eigenstates), and we probe the localized states with single site excitation. After a propagation distance of $1000 \mu\text{m}$, the evolution pattern distributions are illustrated in Fig. 3. The experimental data demonstrates remarkable agreement with the theoretical

simulation results (shown as blank bars in the figure), confirming the exponential localization in the excited site. Moreover, we also inject light into the 4th waveguide, to probe the extended state. This particular injection position is chosen since the site has a large overlap with the two extended eigenstates, survived at such larger potential (also shown in Supplementary Information E). Both linear and logarithmic scale intensity distributions are exhibited in Fig. 3, and clearly depict a marked contrast to the localized states in terms of light evolution patterns. Our results prove the coexistence of energy-dependent localized and extended states induced by multiple MEs in the $\kappa = 3$ mosaic model.

We further confirm the existence of the ME by scanning the quasiperiodic modulation strength in a $\kappa = 2$ mosaic lattice and investigating the critical state near ME. As shown in Fig. 4(a), we first locate the 14th eigenstate in the energy diagram. As we vary the modulation strength from $\lambda = 1.5$ to 5, this eigenstate consistently remains close to the upper ME. Considering the spatial intensity distribution of the eigenstate, we select lattice site 21 as the excitation site due to its larger overlap, and analyze the weights of different eigenenergies by projecting the evolution pattern over all 21 eigenstates. Notably, the weight analysis is time-independent when calculating with state vectors. However in our case, since the phase information is missing during the intensity measurement, we choose a relatively small propagation distance as $100 \mu\text{m}$ to make the phase change negligible, such experimental condition allows us to mimic a delta function excitation. We measure five samples with different modulation potentials and record all the intensity distributions

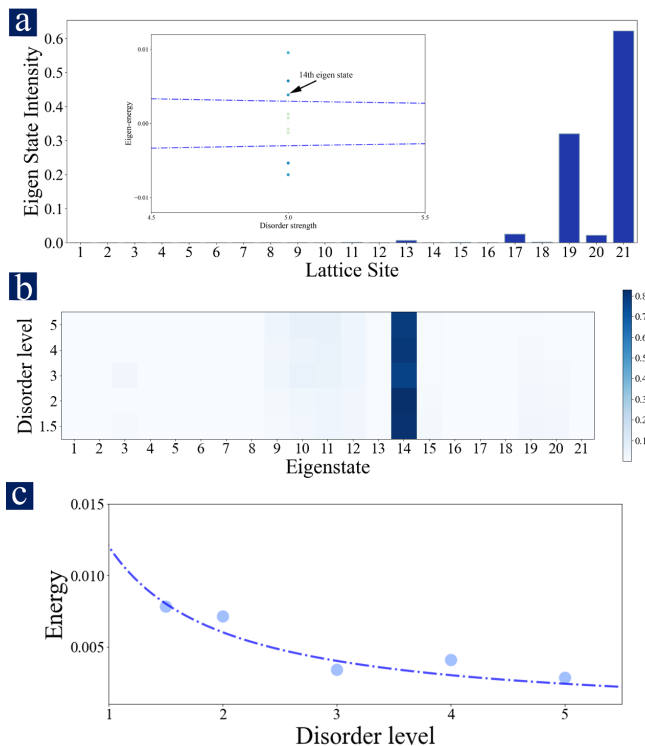


FIG. 4. **Probing the mobility edge in $\kappa = 2$ mosaic lattice.** Panel (a) illustrates the spatial distribution of the 14th eigenstate, which is found to have a significant overlap with the 21st lattice site. This specific site is chosen for the application of single site excitation to effectively probe the system. The overlaid inset provides a detailed view of this eigenstate's relative location in the broader energy spectrum. It is noted that this eigenstate resides in close proximity to the exact ME, as determined by the theoretical model. The critical energy E_c is given by $E_c = \frac{J}{\lambda}$, wherein the ME occurs. A number of samples are fabricated with varying degrees of disorder strength and then subsequently probed for the presence of the 14th eigenstate near the ME. (b) The color map presents the weight overlap analysis between the eigenstates and the output intensity distribution, obtained experimentally following the single-site excitation at the 21st waveguide and after the wave has propagated a distance of $100 \mu\text{m}$ through the lattice structure. It is observed that the output intensity distribution shows a considerable overlap with the 14th eigenstate, positioned near the ME across a range of disorder strengths. (c) The final plot shows the constructed energy level of the experimental excitation for various disorder strengths, the measured energy conforms to the ME within the system, thus providing further evidence for the transition between extended and localized states in the mosaic lattice. The points represent the experimentally measured data, while the line shows analytical ME, Eq. (5).

$\{I^{exp}\}$. The weight $\{w_i\}$ for each sample is given by $w_i = |\langle \psi_i | \sqrt{I^{exp}} \rangle|^2$, where $|\psi_i\rangle$ represents the i -th eigenstate under the corresponding potential. The calculated results in Fig. 4(b) clearly show the excitation state maintains a dominant overlap with the 14th eigenstate while scanning the disorder level. Based on the weight analysis, we estimate the energy of the excitation state $E_{ex} = \sum_i w_i E_i$ with different modulation amplitudes. These values are depicted in the energy spectrum

shown in Figure 4(c), which follow the trend of the $\kappa = 2$ ME as the strength of the quasiperiodic potential increases.

In conclusion, we have experimentally implemented a novel class of quasiperiodic mosaic lattices, offering a crucial advancement in the quest for understanding ME physics. Leveraging integrated photonics platforms, we could design and realize the mosaic lattices in a scalable and flexible fashion with fast prototype. We could effectively probe the intricate behaviour of coexistence of localized and extended states in the mosaic model, revealing crucial insights into the energy-dependent localization transition. Our work demonstrates that quasiperiodic mosaic systems indeed exhibit richer physics than well appreciated random disorder models, substantially extending our understanding of the mechanisms driving phase transitions in disordered systems. Our findings, therefore, underscore a significant advancement in the field, with the potential to catalyze new research directions in quantum physics, materials science, and beyond.

Acknowledgments

A.W.E acknowledges support Knut and Alice Wallenberg (KAW) Foundation through the Wallenberg Centre for Quantum Technology (WACQT), Swedish Research Council (VR) Starting Grant (Ref: 2016-03905), and Vinnova quantum kick-start project 2021. V.Z. acknowledges support from the KAW and VR. Work at Nordita was supported by European Research Council under the European Union Seventh Framework ERS-2018-SYG HERO, KAW 2019.0068 and the University of Connecticut.

* junga@kth.se; These authors contributed equally to this work
 † ivan.khaymovich@gmail.com; These authors contributed equally to this work
 ‡ elshaari@kth.se

- [1] P. W. Anderson, Absence of diffusion in certain random lattices, *Phys. Rev.* **109**, 1492 (1958).
- [2] P. A. Lee and T. V. Ramakrishnan, Disordered electronic systems, *Rev. Mod. Phys.* **57**, 287 (1985).
- [3] B. Kramer and A. MacKinnon, Localization: theory and experiment, *Rep. Prog. Phys.* **56** 1469 (1993).
- [4] E. Abrahams, P. W. Anderson, D. C. Licciardello and T. V. Ramakrishnan, Scaling theory of localization: absence of quantum diffusion in two dimensions, *Phys. Rev. Lett.* **42**, 673 (1979).
- [5] F. Evers and A. D. Mirlin, Anderson transitions, *Rev. Mod. Phys.* **80**, 1355 (2008).
- [6] S. Aubry and G. André, Analyticity breaking and Anderson localization in incommensurate lattices, *Ann. Israel Phys. Soc* **3**, 133 (1980).
- [7] P. G. Harper, Single band motion of conduction electrons in a uniform magnetic field, *Proc. Phys. Soc., London Sect. A* **68**, 874 (1955).

- [8] Y. Lahini, R. Pugatch, F. Pozzi, M. Sorel, R. Morandotti, N. Davidson and Y. Silberberg, Observation of a localization transition in quasiperiodic photonic lattices, *Phys. Rev. Lett.* **103**, 013901 (2009).
- [9] G. Roati, C. D’Errico, L. Fallani, M. Fattori, C. Fort, M. Zaccanti, G. Modugno, M. Modugno and M. Inguscio, Anderson localization of a non-interacting Bose–Einstein condensate, *Nature* **453**, 895 (2008).
- [10] L. Fallani, J. E. Lye, V. Guarrera, C. Fort and M. Inguscio, Ultracold atoms in a disordered crystal of light: towards a Bose glass, *Phys. Rev. Lett.* **98**, 130404 (2007).
- [11] R. E. Prange, D. R. Grempel and S. Fishman, Wave functions at a mobility edge: An example of a singular continuous spectrum, *Phys. Rev. B* **28**, 7370 (1983).
- [12] J. Biddle, B. Wang, D. J. Priour Jr and S. Das Sarma, Localization in one-dimensional incommensurate lattices beyond the Aubry–André model, *Phys. Rev. A* **80**, 021603(R) (2009).
- [13] J. Biddle and S. Das Sarma, Predicted mobility edges in one-dimensional incommensurate optical lattices: an exactly solvable model of Anderson localization, *Phys. Rev. Lett.* **104**, 070601 (2010).
- [14] S. Gopalakrishnan, Self-dual quasiperiodic systems with power-law hopping, *Phys. Rev. B* **96**, 054202 (2017).
- [15] X. Deng, S. Ray, S. Sinha, G. V. Shlyapnikov and L. Santos, One-dimensional quasicrystals with power-law hopping, *Phys. Rev. Lett.* **123**, 025301 (2019).
- [16] M. Saha, S. K. Maiti and A. Purkayastha, Anomalous transport through algebraically localized states in one dimension, *Phys. Rev. B* **100**, 174201 (2019).
- [17] G. L. Celardo, R. Kaiser and F. Borgonovi, Shielding and localization in the presence of longrange hopping, *Phys. Rev. B* **94**, 144206 (2016).
- [18] X. Deng, V. E. Kravtsov, G. V. Shlyapnikov and L. Santos, Duality in power-law localization in disordered one-dimensional systems, *Phys. Rev. Lett.* **120**, 110602 (2018).
- [19] P. A. Nosov, I. M. Khaymovich and V. E. Kravtsov, Correlation-induced localization, *Phys. Rev. B* **99**, 104203 (2019).
- [20] P. A. Nosov and I. M. Khaymovich, Robustness of delocalization to the inclusion of soft constraints in long-range random models, *Phys. Rev. B* **99**, 224208 (2019).
- [21] A. G. Kutlin and I. M. Khaymovich, Renormalization to localization without a small parameter, *SciPost Phys.* **8**, 049 (2020).
- [22] X. Deng, A. L. Burin and I. M. Khaymovich, Anisotropy-mediated reentrant localization, *SciPost Phys.* **13**, 116 (2022).
- [23] A. K. Das and A. Ghosh, Nonergodic extended states in the β ensemble, *Phys. Rev. E* **105**, 054121 (2022).
- [24] A. K. Das, A. Ghosh, and I. M. Khaymovich, Absence of mobility edge in short-range uncorrelated disordered model: Coexistence of localized and extended states (2023), arXiv:2305.02351 [cond-mat.dis-nn].
- [25] S. Das Sarma, S. He and X. C. Xie, Mobility edge in a model one-dimensional potential, *Phys. Rev. Lett.* **61**, 2144 (1988).
- [26] S. Das Sarma, S. He and X. C. Xie, Localization, mobility edges, and metal-insulator transition in a class of one-dimensional slowly varying deterministic potentials, *Phys. Rev. B* **41**, 5544 (1990),
- [27] S. Ganeshan, J. H. Pixley and S. Das Sarma, Nearest neighbor tight binding models with an exact mobility edge in one dimension, *Phys. Rev. Lett.* **114**, 146601 (2015).
- [28] X. Li, X. Li and S. Das Sarma, Mobility edges in one dimensional bichromatic incommensurate potentials, *Phys. Rev. B* **96**, 085119 (2017).
- [29] H. Yao, H. Khoudli, L. Bresque and L. Sanchez-Palencia, Critical behavior and fractality in shallow one-dimensional quasiperiodic potentials, *Phys. Rev. Lett.* **123**, 070405 (2019).
- [30] H. Yin, J. Hu, A.-C. Ji, G. Juzeliunas, X.-J. Liu and Q. Sun, Localization driven superradiant instability, *Phys. Rev. Lett.* **124**, 113601 (2020).
- [31] S. Roy, I. M. Khaymovich, A. Das and R. Moessner, Multifractality without fine-tuning in a Floquet quasiperiodic chain, *SciPost Phys.* **4**, 025 (2018).
- [32] C. Danieli, J. D. Bodyfelt, and S. Flach, Flat-band engineering of mobility edges, *Phys. Rev. B*, **91**, 235134 (2015).
- [33] A. Ahmed, A. Ramachandran, I. M. Khaymovich and A. Sharma, Flat band based multifractality in the all-band-flat diamond chain, *Phys. Rev. B* **106**, 205119 (2022).
- [34] S. Lee, A. Andreanov and S. Flach, Critical-to-insulator transitions and fractality edges in perturbed flat bands, *Phys. Rev. B* **107**, 014204 (2022).
- [35] Y. Kim, T. Čadež, A. Andreanov and S. Flach, Flat band induced metal-insulator transitions for weak magnetic flux and spin-orbit disorder, *Phys. Rev. B* **107**, 174202 (2023).
- [36] H. P. Lüschen, S. Scherg, T. Kohlert, M. Schreiber, P. Bordia, X. Li, S. Das Sarma and I. Bloch, Single-particle mobility edge in a one-dimensional quasiperiodic optical lattice, *Phys. Rev. Lett.* **120**, 160404 (2018).
- [37] F. A. An, K. Padavić, E. J. Meier, S. Hegde, S. Ganeshan, J. H. Pixley, S. Vishveshwara and B. Gadway, Interactions and mobility edges: observing the generalized Aubry–André model, *Phys. Rev. Lett.* **126**, 040603 (2021).
- [38] Y. Wang, J.-H. Zhang, Y. Li, J. Wu, W. Liu, F. Mei, Y. Hu, L. Xiao, J. Ma, C. Chin and S. Jia, Observation of interaction-induced mobility edge in an atomic Aubry–André wire, *Phys. Rev. Lett.* **129**, 103401 (2022).
- [39] A. Avila, Global theory of one-frequency Schrödinger operators, *Acta. Math.* **1**, 215 (2015).
- [40] Y. Wang, X. Xia, L. Zhang, H. Yao, S. Chen, J. You, Q. Zhou and X.-J. Liu, One-dimensional quasiperiodic mosaic lattice with exact mobility edges, *Phys. Rev. Lett.* **125**, 196604 (2020).
- [41] L. Lu, J. D. Joannopoulos and M. Soljacic, Topological photonics, *Nat. Photonics* **8**, 821 (2014).
- [42] T. Ozawa, H. M. Price, A. Amo, N. Goldman, M. Hafezi, L. Lu, M. C. Rechtsman, D. Schuster, J. Simon, O. Zilberberg and I. Carusotto, Topological photonics, *Rev. Mod. Phys.* **555**, 015006 (2019).
- [43] D. Smirnova, D. Leykam, Y. Chong and Y. Kivshar, Nonlinear topological photonics, *Appl. Phys. Rev.* **7**, 021306 (2020).
- [44] D. T. H. Tan, Topological silicon photonics, *Adv. Photonics Res.* **2**, 2100010 (2021).
- [45] J. Wang, F. Sciarrino, A. Laing and M. G. Thompson, Integrated photonic quantum technologies, *Nat. Photonics* **14**, 273 (2020).
- [46] A. W. Elshaari, W. Pernice, K. Srinivasan, O. Benson and V. Zwiller, Hybrid integrated quantum photonic circuits, *Nat. Photonics* **14**, 285 (2020).
- [47] G. Moody, V. J. Sorger, D. J. Blumenthal, P. W. Juodawlkis, W. Loh, C. Sorace-Agaskar, A. E. Jones, K. C. Balram, J. C. Matthews, A. Laing, M. Davanco, L. Chang, J. E. Bowers, N. Quack, C. Galland, I. Aharonovich, M. A. Wolff, C. Schuck, N. Sinclair, M. Loncar, T. Komljenovic, D. Weld, S. Mookherjee, S. Buckley, M. Radulaski, S. Reitzenstein, B. Pingault, B. Machielse, D. Mukhopadhyay, A. Akimov, A. Zheltikov, G. S. Agarwal, K. Srinivasan, J. Lu, H. X. Tang, W. Jiang, T. P. McKenna, A. H. Safavi-Naeini, S. Steinhauer, A.

- W. Elshaari, V. Zwiller, P. S. Davids, N. Martinez, M. Gehl, J. Chiaverini, K. K. Mehta, J. Romero, N. B. Lingaraju, A. M. Weiner, D. Peace, R. Cernansky, M. Lobino, E. Diamanti, L. T. Vidarte and R. M. Camacho, 2022 Roadmap on integrated quantum photonics, *Journal of Physics: Photonics* **4**,1, 012501 (2022).
- [48] J. Chang, J. Gao, I. Esmail Zadeh, A. W. Elshaari and V. Zwiller, Nanowire-based integrated photonics for quantum information and quantum sensing, *Nanophotonics* **12**, 339 (2023).
- [49] Y. Lahini, Y. Bromberg, D. N. Christodoulides and Y. Silberberg, Quantum correlations in two-particle Anderson localization, *Phys. Rev. Lett.* **105**, 163905 (2010).
- [50] M. Segev, Y. Silberberg and D. N. Christodoulides, Anderson Localization of Light, *Nat. Photonics* **7**, 197 (2013).
- [51] A. Crespi, R. Osellame, R. Ramponi, V. Giovannetti, R. Fazio, L. Sansoni, F. De Nicola, F. Sciarrino and P. Mataloni, Anderson localization of entangled photons in an integrated quantum walk, *Nat. Photonics* **7**, 322–328 (2013).
- [52] L. Chrostowski and M. Hochberg, *Silicon Photonics Design: From Devices to Systems*. (Cambridge University Press, 2015).
- [53] FDTD: 3D Electromagnetic Simulator, *Lumerical Inc.*
- [54] J. Gao, Z.-S. Xu, D. A Smirnova, D. Leykam, S. Gyger, W.-H. Zhou, S. Steinhauer, V. Zwiller and A. W. Elshaari, Observation of Anderson phase in a topological photonic circuit, *Phys. Rev. Research* **4**, 033222 (2022).
- [55] Z.-S. Xu, J. Gao, G. Krishna, S. Steinhauer, V. Zwiller and A. W. Elshaari, Direct measurement of topological invariants in photonic superlattices, *Photon. Res.* **10**, 2901-2907 (2022).
- [56] J. Gao, L. Santos, G. Krishna, Z.-S. Xu, A. Iovan, S. Steinhauer, O. Gühne, P. Poole, D. Dalacu, V. Zwiller and A. W. Elshaari, Scalable generation and detection of on-demand W states in nanophotonic circuits, *Nano Letters* **23**, 5350-5357 (2023).